Opt Rev (2016) 23:26–32
DOI 10.1007/s10043-015-0153-y

REGULAR PAPER

A non-contact FBG vibration sensor with double differential temperature compensation

Tianliang Li[1] · Yuegang Tan[1] · Zude Zhou[1] · Kai Zheng[1]

Received: 24 June 2015 / Accepted: 2 November 2015 / Published online: 18 November 2015

Abstract This paper has presented a non-contact fiber Bragg grating (FBG) vibration sensor with double differential temperature compensation. Two FBGs and two states of the sensor have been employed to achieve double differential temperature compensation. Based on magnetic coupling and FBG sensing principle, it can be used to realize non-contact measurement of vibration of the rotating shaft. Experimental results show that the working band ranges are within 0–150 Hz; the sensitivity is −0.67 pm/μm, and the linearity is 3.87 % within a range of 2–2.6 mm. The fitting equation of temperature compensation which is caused by structural inflation can be expressed as: $\Delta\lambda_1' - \Delta\lambda_2' = 1.51 \times T - 32.97$. When used to amend a temperature error, the sensor's temperature error will be reduced to 1.19 % in the range of 25–60 °C.

Keywords Double differential · Temperature compensation · Vibration sensor · FBG

1 Introduction

Optical fiber Bragg grating (FBG) sensors have aroused people's attention in the sensing field these years. They are resistant to electromagnetic interference (EMA), high reliability, small volume, and especially suitable for using the strong magnetic, radioactive and corrosive field. And it is the most promising optical sensor now [1, 2]. There are many related reports about design and application of vibration sensors based on FBG sensing. Zhou et al. considered cantilever beam as an elastomer, and symmetrically pasted FBGs on the upper and the bottom surface of the beam to design vibration sensor [3]; Antunes et al. made L shaped beam as an elastomer of vibration sensor, mixed the mass on the end of beam which was supported by spring, and the another end beam was connected by FBG, to achieve dynamic monitoring of the structure vibration [4]; Weng et al. also combined diaphragm with L shaped rigid beam to design a contact type of acceleration sensor to monitor structure health and earthquake [5]; Liu et al. used flat diaphragm as elastic body, added a mass block in the center of flat diaphragm, through the inertia force of mass caused the flat diaphragm deformation, and then obtained the vibration acceleration of measured body [6]; literature [7, 8] have proposed a kind of FBG based on non-contact magnetic coupling displacement/vibration sensor, to achieve non-contact measurement for the objects.

For the above vibration sensors, they have a common problem which is the temperature coupling. When the temperature cross sensitivity of vibration sensors is eliminated, the measurement accuracy will be enhanced. At present, some scholars used many kinds of methods to deal with this issue. Such as Wang et al. made the two FBGs difference to realize temperature compensation, which are symmetry pasted the FBGs on the up and down surface of beam [9]; Huang et al. used the different thermal expansion coefficient materials to encapsulate the FBG sensors, which greatly reduced the temperature influence; finally, the temperature sensitivity was about 1/23 of non-temperature compensation sensor [10]; Iwashima et al. adopted a new encapsulation technology, using liquid crystal polymer pipe to pack the FBGs; its temperature sensitivity could be decreased to 0.13 nm/100 °C [11]. The above methods indeed decreased the temperature cross sensitivity of

✉ Tianliang Li
tianliangliwhut@sina.com

[1] Wuhan University of Technology, Wuhan 430070, Hubei, China

sensors in a certain extent, but these methods are more complex, the structure is not easy to process and ranges of temperature compensation are limited. Therefore, it is necessary to propose a simple method to eliminate temperature compensation for the FBG vibration sensor.

This paper has proposed a non-contact FBG vibration sensor with double differential temperature compensation. We used 2 FBGs and 2 different states of the sensor to achieve the double differential temperature compensation. Based on magnetic coupling and FBG sensing principle, it can be used to realize non-contact measurement of the vibration of a rotating shaft. The working principle of the sensor with temperature compensation has been analyzed by theory in this article. The paper is mainly divided into the following parts: the basic principle and model of sensors, the temperature compensation principle of sensor, sensor's sensing characteristic, experiments analysis and the double differential temperature compensation experiment analysis.

2 Model and principle of the sensor

According to the sensing principle of FBG, when a broadband incident light enters into the optical fiber and meets the FBG, a specific wavelength narrow band light will be reflected. When the FBG is stretched/compressed or its environment temperature changes, these factors will cause the grating period Λ and effective refractive index n_{eff} of FBG changes. So the relation between strain/temperature and center wavelength shifts can be described by

$$\frac{\Delta\lambda_B}{\lambda_B} = (1-\rho_e)\Delta\varepsilon + (\alpha_n + \alpha_A)\Delta T \tag{1}$$

where $\Delta\lambda_B$ is the center wavelength shifts, λ_B is the center wavelength of FBG, $\Delta\varepsilon$ is the strain, ρ_e is the strain optic coefficient of an optical fiber, and ΔT is the increment of temperature.

2.1 Principle of sensor

The principle of the sensor is shown in Fig. 1. According to the magnetic coupling of the permanent magnet on the measured magnetic shaft, when the rotating shaft vibrates, the distance between permanent magnets and measured shaft will change, also it will make the diaphragm deformation vary. And then the #1FBG's center wavelength will be changed under tension/compression force. Therefore, through the #1FBG's center wavelength shifts, we can achieve the vibration of the rotating shaft.

When the sensor works in a various environmental temperature, both FBGs are directly interfered by the temperature. So we can use the two FBGs difference to eliminate the direct temperature influence of the #1FBG, then the #1FBG's center wavelength is only interfered by the structure thermal expansion stress and the magnetic force at working. When the sensor is not working, we only change the environment temperature, and then use the two FBGs difference to eliminate the direct temperature influence of the #1FBG; their strain will not be interfered by the magnetic force. So we can use the two states (working/not working) differential to reduce structure thermal expansion error. Finally, we can use the double differential method to eliminate the temperature error.

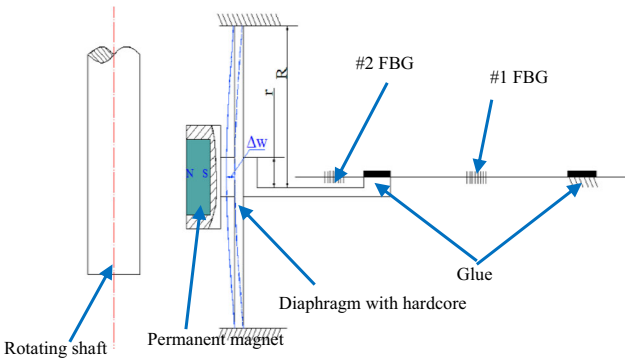

Fig. 1 Equivalent structure model of sensor

In the working condition, we can find that there are three factors causing the center wavelength shifts of #1 FBG, which are magnetic force, temperature directly effect and structure thermal expansion of sensor. $\Delta\varepsilon$ is mainly consisting of diaphragm deformation Δw and structure linear expansion ΔL, so we can get the relationship between the $\Delta\varepsilon$ and Δw, ΔL:

$$\Delta\varepsilon = \frac{\Delta w}{L} + \frac{\Delta L}{L} \tag{2}$$

where Δw is the bending deflection of diaphragm hardcore, ΔL is the length of structure linear expansion, and L is the effective working length of the #1FBG.

Combining Eqs. (1) and (2), the center wavelength shifts of #1FBG can be described as:

$$\frac{\Delta\lambda_1}{\lambda_1} = (1-\rho_e)\frac{\Delta w}{L} + (1-\rho_e)\frac{\Delta L}{L} + (\alpha_n + \alpha_A)\Delta T \tag{3}$$

When the environment temperature of the sensor changes, the linear expansion length of diaphragm will change less compared with the other parts of the sensor. Because the diaphragm's thickness is very thin, so we can ignore the temperature influence of diaphragm. The FBG's center wavelength shifts are only affected by the lateral deformation of the base in the expansion processing, so we can simplify the bases' linear expansion model of #1 FBG and #2FBG which is shown in Fig. 2.

According to the expansion properties of the material, we can get the relationships between linear expansion

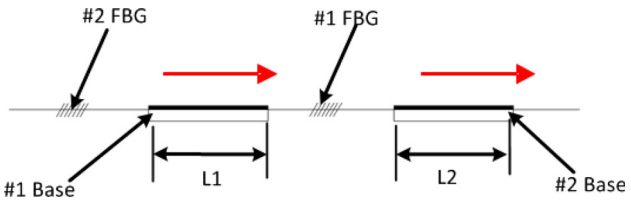

Fig. 2 Structure expand equivalent model of sensor

length # 1 and # 2 base and temperature are separately as following:

$$\Delta L_1 = \alpha_1 L_1 \Delta T \quad \Delta L_2 = \alpha_2 L_2 \Delta T \tag{4}$$

$$\Delta L = (\alpha_1 L_1 - \alpha_2 L_2)\Delta T \tag{5}$$

where α_1 is the linear thermal expansion coefficient of #1 base, α_2 is the linear thermal expansion coefficient of #2 base, L_1 is the length of #1 base, and L_2 is the length of #1 base.

According to the Eqs. (3–5), the Eq. (3) can be rewritten as:

$$\frac{\Delta\lambda_1}{\lambda_1} = (1-\rho_e)\frac{\Delta w}{L} + (1-\rho_e)\frac{(\alpha_1 L_1 - \alpha_2 L_2)\Delta T}{L} + (\alpha_n + \alpha_A)\Delta T \tag{6}$$

2.2 Double FBGs difference

Due to the #2FBG is suspended in the inside of structure, so it is only affected by temperature. The relationship between #2FBG's center wavelength shifts and the temperature can be expressed by Eq. (8):

$$\frac{\Delta\lambda_2}{\lambda_2} = (\alpha_n + \alpha_A)\Delta T \tag{7}$$

According to the double FBGs' difference principle, we use the Eq. (6) to minus Eq. (7), it can easily eliminate the temperature cross sensitivity which is the direct coupling effect of the # 1 FBG. The equation can be simplified as:

$$\frac{\Delta\lambda_1}{\lambda_1} - \frac{\Delta\lambda_2}{\lambda_2} = (1-\rho_e)\frac{\Delta w}{L} + (1-\rho_e)\frac{(\alpha_1 L_1 - \alpha_2 L_2)\Delta T}{L} \tag{8}$$

2.3 Working status of difference

When the sensor is not working, the # 1 FBG will be affected by temperature and structure thermal expansion, so the Eq. (8) can be written as:

$$\frac{\Delta\lambda_1'}{\lambda_1} - \frac{\Delta\lambda_2'}{\lambda_2} = (1-\rho_e)\frac{(\alpha_1 L_1 - \alpha_2 L_2)\Delta T}{L} \tag{9}$$

Combining the Eqs. (8) and (9), we can get a matrix, which can be expressed as:

$$\begin{bmatrix} \frac{\Delta\lambda_1}{\lambda_1} - \frac{\Delta\lambda_2}{\lambda_2} \\ \frac{\Delta\lambda_1'}{\lambda_1} - \frac{\Delta\lambda_2'}{\lambda_2} \end{bmatrix} = \begin{bmatrix} \frac{1-\rho_e}{L} & (1-\rho_e)\frac{(\alpha_1 L_1 - \alpha_2 L_2)}{L} \\ 0 & (1-\rho_e)\frac{(\alpha_1 L_1 - \alpha_2 L_2)\Delta T}{L} \end{bmatrix} \begin{bmatrix} \Delta w \\ \Delta T \end{bmatrix} \tag{10}$$

We use the first row of the matrix to minus the second row; a new equation can be given as:

$$\frac{\Delta\lambda_1 - \Delta\lambda_1'}{\lambda_1} - \frac{\Delta\lambda_2 - \Delta\lambda_2'}{\lambda_2} = (1-\rho_e)\frac{\Delta w}{L} \tag{11}$$

The relationship between the diaphragm deformation Δw and air gap spacing L_g can be achieved from the literature [8]. And combining the Eq. (11), we can find that $\frac{\Delta\lambda_1 - \Delta\lambda_1'}{\lambda_1} - \frac{\Delta\lambda_2 - \Delta\lambda_2'}{\lambda_2}$ is only related to L_g, so the direct or indirect coupling error of temperature will be eliminated. Although the relationship between the center wavelength shift and the air gap spacing L_g is nonlinearity, we can make the linear fitting in a certain range. Finally, the vibration of the rotating shaft can be measured by the FBGs center wavelength shift with temperature compensation.

3 Sensing characteristics experiments

The physical map of the sensor is shown in Fig. 3. The diaphragm's attributes are as follows: the radius $R = 3$ mm, hard heart radius $r = 1.5$ mm, the thickness $h = 0.05$ mm; NdFeB (neodymium iron boron) cylindrical permanent magnet is N35 (outer diameter is 10 mm, length is 10 mm). The # 1 FBG initial center wavelength is 1285.834 nm, and # 2 FBG initial center wavelength is 1315.542 nm under the room temperature.

Fig. 3 Physical map of sensor

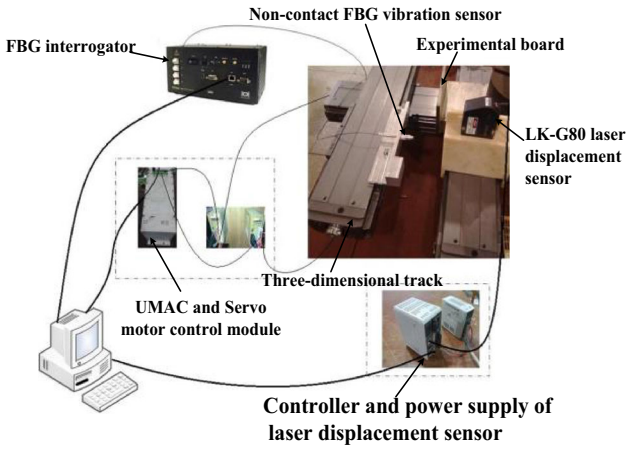

Fig. 4 Schematic diagram of the static experiment system

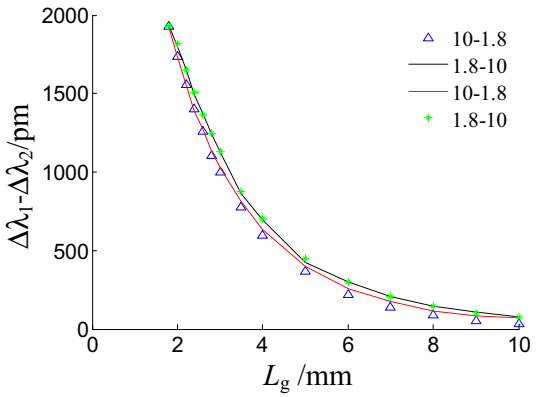

Fig. 5 Center wavelength shift $\Delta\lambda$ versus air gap spacing L_g in the range from 1.8–10 mm

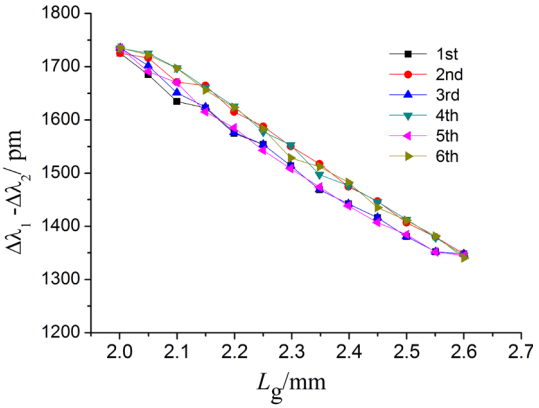

(a) Center wavelength shift $\Delta\lambda$ versus air gap spacing L_g in the range from 2~2.6mm

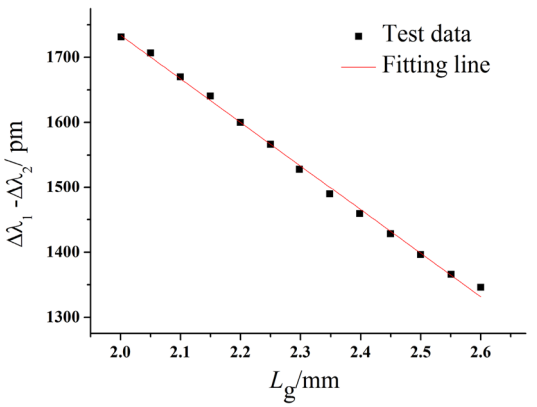

(b) The linear fitting curve

Fig. 6 The relationship between center wavelength shift $\Delta\lambda$ and air gap spacing L_g

3.1 Static characteristics experiment

Static characteristics are the sensor's the basic performance. We built the static experiment system (Fig. 4) which consists mainly of the LK-G80 laser displacement sensor (reference distance 80 mm; range ±15 mm; repeatability 0.2 μm; linearity ±0.05 %) and three-dimensional track. During the experiment, firstly, we used the PC to send the instructions to the UMAC controller, and made the servo motor drive the three-dimensional track, then used the LK-G80 laser displacement sensor to ensure the distance which is between the sensor and the experimental board, and finally we could use the FBG interrogator to acquire the signal and save them by the computer. So long as we repeated the above steps, and constantly adjusted the air gap spacing L_g, the static characteristics of the sensor can be easily achieved.

Through adjusting the three-dimensional track, the air gap spacing can be changed within 1.8–10 mm in this experiment. We repeated the experiment 4 times. Figure 5 shows the relation between the shifts of center wavelength of FBG and air gap spacing, which is basically consistent with the Eq. (11). From this figure, it is easily get that when the L_g resides in 1.8–3 mm, the sensitivity of the sensor is better compared with the other zones.

We chose the 2–2.6 mm as the working range of the sensor. The first picture in Fig. 6 shows the $\Delta\lambda$ versus L_g in the range from 2 to 2.6 mm. The experiment has been repeated for 6 times. From this picture, the repeatability error of sensor is 9.08 %. Figure 6b shows the average difference value of wavelength shifts,which is obtained in the repeated experiments. From the fitting straight line in Fig. 6b, we can obtain the following properties of sensor: (1) fitted equation: $\Delta\lambda_1 - \Delta\lambda_2 = -671.4 \times L_g + 3077.3$, (2) sensor's sensitivity: −0.67 pm/μm, (3) linearity: 3.87 %, (4) linear fitting correlation coefficient: 0.9974.

3.2 Dynamic properties experiment

In order to study on dynamic properties of sensor, we set up the dynamic experimental system (Fig. 7), which is mainly composed of "B&K4808" vibration test systems,

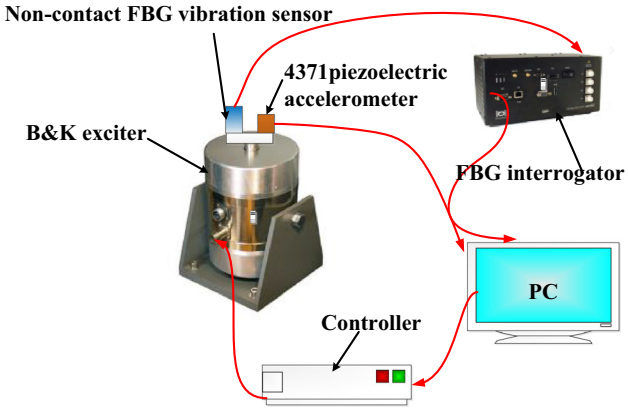

Fig. 7 The schematic of dynamic experiment system

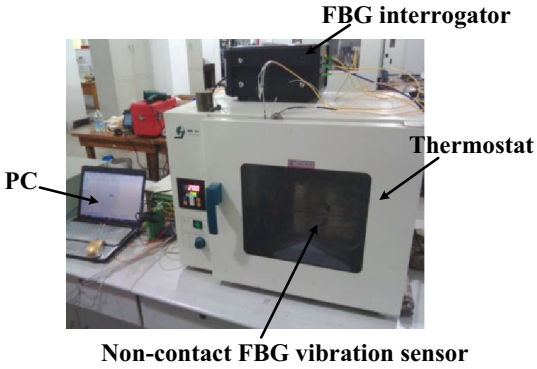

Fig. 9 Temperature compensation of structure thermal expansion experimental system

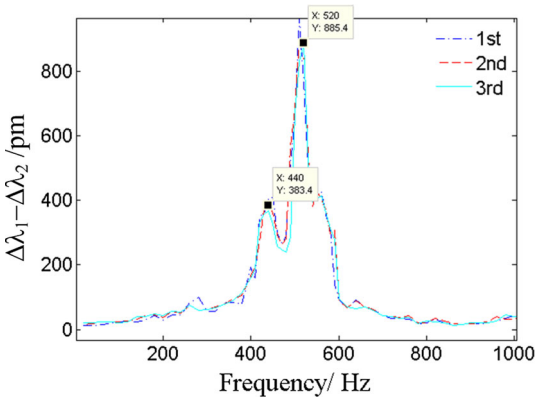

Fig. 8 Amplitude–frequency curve of the sensor

"B&K"4371piezoelectric accelerometer and FBG interrogator, et al. We sent the orders to the controller to adjust the frequency or amplitude of the exciter. The acceleration amplitude was set at 2 g, and sinusoidal signal frequency ranged from 50 to 2000 Hz. The experiment was repeated 3 times. So we can obtain the Fig. 8, which shows the amplitude frequency characteristic curve of the sensor. When the frequency is (1) within 0–150 Hz, the curve is almost parallel to *x* axis, so the working band of the sensor is 0–150 Hz; (2) equal to 520 Hz, the center wavelength shifts are reaching the maximum, so the resonant frequency of the sensor is 520 Hz.

4 Double differential temperature compensation experiment

In the temperature compensation experiment, we used the thermostat to control the around environment temperature of the sensor (Fig. 9). Due to the static characteristics, experiment of the sensor was attained at room temperature in this paper, so we controlled the temperature start from

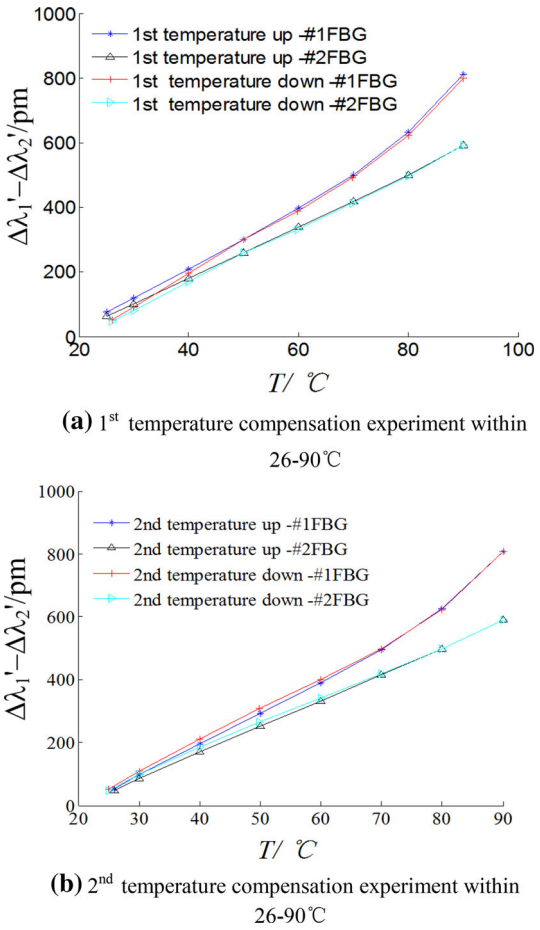

(a) 1st temperature compensation experiment within 26-90℃

(b) 2nd temperature compensation experiment within 26-90℃

Fig. 10 The two FBGs' center wavelength shifts versus temperature

25 °C in this experiment. We have set the interval as 10 °C in the range from 30 to 90 °C, and used the FBG interrogator acquired and stored the signals. The experiment was repeated 4 times.

The two FBGs' center wavelength shifts versus temperature are shown in Fig. 10. From the figure, we can find that when the temperature is within 25 to 90 °C, the center

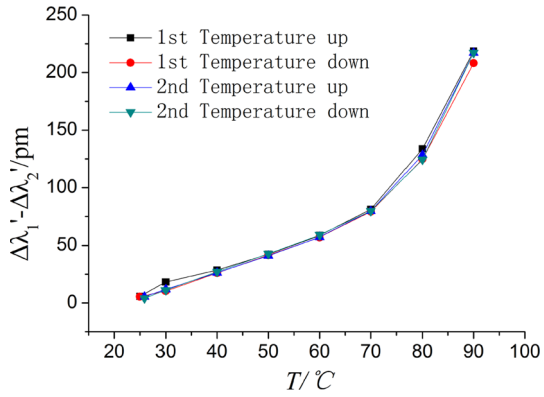

Fig. 11 #1 FBG center wavelength shift caused by structure thermal expansion

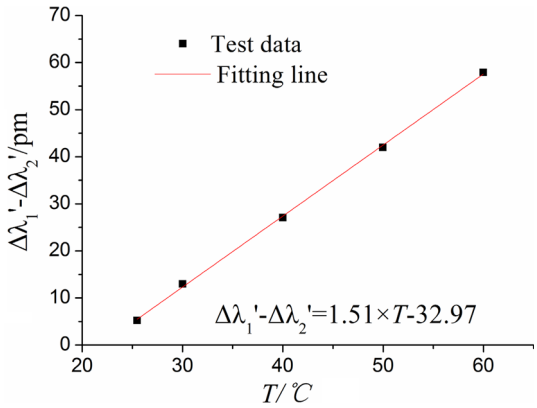

Fig. 12 The fitting curve of #1 FBG center wavelength shift caused by structure thermal expansion within 25–60 °C

wavelength shifts of the #1FBG are bigger than the #2FBG. Because the #1FBG is stretched by the thermal expansion stress of structure besides effected by temperature. When the temperature is (1) within 25–70 °C, the relationship between the structure thermal expansion stress and temperature curve is almost linear; (2) >70 °C, compared with the 25–70 °C, the #1FBG's center wavelength shifts increase obviously, because the linear expansion coefficient of the material is not a constant in the various temperature range, which is consistent with the above theory.

When we used the value of #1FBG center wavelength shifts value to minus value of #2FBG, we could easily eliminate temperature direct coupling effect on the #1 FBG, and the difference value is only caused by the thermal expansion stress of structure which is shown in Fig. 11. From the figure, we can obviously find that the thermal expansion coefficient of the material can be considered as a constant in the specific scope, which is consistent with its theoretical model. When the temperature exceeds 70 °C, the slope is bigger than in the range of 25–70 °C. So we selected the range from 25 to 60 °C as working environment temperature of sensor. Test data and the fitting line of sensor are shown in Fig. 12. From this figure, we could get the following data: (1) fitted equation: $\Delta\lambda_1' - \Delta\lambda_2' = 1.51 \times T - 32.97$, (2) sensitivity of the structure thermal expansion: 1.51 pm/ °C, (3) linearity: 1.19 %, (4) linear fitting correlation coefficient: 0.9995.

After using the above fitting equation to eliminate the influence of temperature cross-sensitivity, the sensor's temperature error will be reduced to 1.19 % within the range of 25–60 °C. We can also repeat sensor's structure thermal expansion temperature compensation experiment many times, and combine the statistics method to get the higher order time of fitting curve, which can be used to achieve greater range of temperature compensation, and weaken the temperature cross-sensitivity influence on the sensor measurement. Therefore, it can be used to achieve the higher precise measurement of the rotating shaft vibration in a variable temperature environment.

5 Conclusions

This paper has presented a non-contact FBG vibration sensor with double differential temperature compensation. The sensing characteristic experiment results show that: (1) the sensor range is 2–2.6 mm; (2) sensitivity −0.67 pm/μm; (3) linearity 3.87 %; (4) linear regression correlation coefficient of 0.9974; (5) repeatability error of 9.08 %; (6) working band: 0–150 Hz, and (7) resonant frequency: 440/520 Hz. Also according to the double differential temperature compensation experiment, we can find that the sensor's temperature error will be reduced to 1.19 % in the range of 25–60 °C after using the fitting equation: $\Delta\lambda_1 - \Delta\lambda_2' = 1.51 \times T - 32.97$ to make the temperature compensation. So it can be used to achieve the higher precise measurement of the rotating shaft vibration in a variable temperature environment. According to the requirements of monitoring rotating shaft vibration, we can improve the non-contact FBG vibration sensor to achieve the different requirements of vibration condition monitoring.

Acknowledgments This project is supported by the National Natural Science Foundation of China (Project No. 51375358).

References

1. Lee, B.: Review of the present status of optical fiber sensors. Opt. Fiber Technol. **9**(2), 57–59 (2003)
2. Hill K.O., Meltz, G.: Fiber Bragg grating technology fundamentals and overview. J. Lightwave Technol. **15**(8), 1263–1276 (1997)
3. Zhou, W., Dong, X., Shen, C., Zhao, C.-L., Chan, C.C., Shum, P.: Temperature-independent vibration sensor with a fiber Bragg

grating. Inc. Microwave Opt. Technol. Lett. **52**(10), 2282–2285 (2010)
4. Antunes, P.F.D.C., Lima, H.F.T., Alberto, N.J., Rodrigues, H., et al.: Optical fiber accelerometer system for structural dynamic monitoring. IEEE Sens. J. **9**(11), 1347–1354 (2009)
5. Weng, Y., Qiao, X., Feng, Z., Hu, M., Zhang, J., Yang, Y.: Compact FBG diaphragm accelerometer based on L-shaped rigid cantilever beam". Chin. Optics Lett. **9**(10), 100604 (2011)
6. Liu, Q.P., Qiao, X.G., Zhao, J.L., et al.: Novel fiber Bragg grating accelerometer based on diaphragm. IEEE Sens. J. **12**(10), 3000–3004 (2012)
7. Ho-kun, M.I., Qiu-ming, N.A.N.: Study on magnetic coupling FBG displacement sensor. In: Proceedings of the 2011 IEEE International Conference on Mechatronics and Automation, August 7–10, Beijing, China (2011)
8. Li, T., Tan, Y., Wei, L., Zhou, Z., Zheng, K., Guo, Y.: A non-contact fiber Bragg grating vibration sensor. Rev. Sci. Instrum. **85**, 015002 (2014)
9. Wang, T., He, D., Wang, Z., Wang, Y.: A novel temperature self-compensation FBG vibration sensor. 3rd Int. Photonics OptoElectron. Meet. J. Phys Conf. Ser. **276**, 012146 (2011)
10. Huang, Y., Li, J., Kai, G., Yuan, S., Dong, X.: Temperature compensation package for fiber Bragg gratings. Microwave Opt. Technol. Lett. **39**(1), 70–72 (2003)
11. Iwashima, T., Inoue, A., Shigematsu, M., Nishimura, M., Hattori, Y.: Temperature compensation technique for fiber Bragg gratings using liquid crystalline polymer tubes. Electron. Lett. **33**(5), 417–419 (1997)